Heliyon 10 (2024) e28236

Contents lists available at ScienceDirect

Heliyon

journal homepage: www.cell.com/heliyon

Research article

Prognostic correlation between specialized capillary endothelial cells and lung adenocarcinoma

Rongchang Zhao [a], Yan Ding [a], Rongbo Han [b], Rongjie Ding [a], Jun Liu [a], Chunrong Zhu [c], Dan Ding [a,*], Minhui Bao [a]

[a] Department of Oncology, Taixing People's Hospital, Taixing, China
[b] Department of Oncology, The Fourth Affiliated Hospital Of Nanjing Medical University, Nanjing, China
[c] Department of Oncology, First Affiliated Hospital of Soochow University, Suzhou, China

ARTICLE INFO

Keywords:
LUAD
Stromal microenvironment
Capillary endothelial cell
Single-cell
Prognosis

ABSTRACT

Background: In-depth analysis of the functional changes occurring in endothelial cells (ECs) involved in capillary formation can help to elucidate the mechanism of tumour vascular growth.
Methods: Appropriate datasets were retrieved from the GEO database to obtain single-cell data on LUAD samples and adjacent normal tissue samples. ECs were selected by an automatic annotation program in R and further subdivided based on reported EC marker genes. Functional changes in different types of capillary ECs were then visualized, and the concrete expression was classified by genetic data in the TCGA. Finally, a prognostic model was constructed to predict immunoinfiltration status, survival and drug therapy effects.
Results: The LUAD data contained in the GSE183219 dataset were suitable for our analysis. After dimensionality reduction analysis and cell annotation, EC general capillary and EC aerocyte subsets as capillary specialized phenotypes showed a series of functional changes in tumour samples, with a total of 108 genes found to undergo functional changes. Use of CellPhoneDB revealed a close interaction of activity between ECs. After integration of TCGA, GSE68465 and GSE11969 datasets, the genes obtained were analysed by cluster analysis and risk model construction, identifying 8 genes. Drug sensitivity, immune cell and molecular differences can be accurately predicted.
Conclusions: EC general capillary and EC aerocyte subsets are recognized capillary ECs in the tumour microenvironment, and the functional changes between them are relevant to the prognosis and treatment of LUAD patients and have the potential to be used in target therapy.

1. Introduction

Genetic alterations that promote changes in cell function and growth are the foundation of tumour development. However, the activity of tumour cells is the basis of tumour progression. As cells are not separate individuals but closely related symbionts, the abnormal function of tumour cells can also lead to functional changes in other types of cells that are not cancerous [1–3]. According to the tumour microenvironment theory, other cell types that surround tumour cells include immune cells and stromal cells, and the former have become increasingly important in many studies [4–7]. Conversely, stromal cells have not received as much attention as

* Corresponding author.
E-mail address: dingdan2993@163.com (D. Ding).

https://doi.org/10.1016/j.heliyon.2024.e28236
Received 30 September 2023; Received in revised form 12 March 2024; Accepted 14 March 2024
Available online 16 March 2024

immune cells; the reason may be that there are many kinds of stromal cells, that there are various combinations of stromal cells in the tissues of each organ, and that each stromal cell has different functions, for example, cancer-associated fibroblasts (CAFs), macrophages, and endothelial cells. The relationship between CAFs and tumours has been gradually clarified [8–11]. Macrophages are the body's defence system, and their role in phagocytic tumour cells has been clearly defined [12]. Endothelial cells (ECs) can be divided into several types according to their function, but their relationship with tumours has not been elucidated. As an important organ of the human body, the lungs are responsible for the respiratory and circulatory systems. ECs play a vital role in lung tissue by serving as a barrier between the air, blood and stromal tissue; they also rely on their metabolic activity to participate in processes such as angiogenesis, inflammation control and white blood cell transport. Lung adenocarcinoma (LUAD) is a type of tumour with a high incidence, and LUAD tumour cells inevitably engage in functional interactions with other cells in the microenvironment during tumour development and metastasis [13]. ECs in lung tissue play important roles in the tumour microenvironment, and other cells can interfere with ECs by affecting physiological activities [14], which may lead to poor treatment response and poor prognosis. Previous studies have neglected the changes that occur in ECs during the occurrence and development of LUAD and the impact on the prognosis of patients. The main manifestations of LUAD are as follows: first, "ECs in the tumour microenvironment" are a general term for a class of cells, and no studies have accurately classified the composing cells; second, "ECs in lung tissue" are involved in many functions, and there is no effective means to sort out these cells; and third, there are no relevant studies on the effects of different differentiation types of homologous ECs on tumour cells.

The advent of single-cell RNA sequencing (scRNA-seq) has made it possible to perform specific analyses of cell populations at the single-cell level. The main principle of scRNA-seq technology is to use detection tools such as integrated microfluidic chips to obtain the contents of individual cells, such as RNA/DNA, proteins, metabolites and other biological macromolecules, through the rupture and release of cell membranes. These inclusions were analysed to more thoroughly elucidate the composition and function of the cells. In contrast to traditional RNA-sequencing (RNA-seq) methods, which process millions of cells and average potential differences, scRNA-seq can reveal the changes that make each cell type unique [15,16]. At present, there are three main methods used to construct single-cell transcriptomes: SMART amplification, 10 × Genomics and Andeplete. Using these techniques and in-depth data analysis, we can determine cell heterogeneity, changes in gene expression, cell–cell interactions, cell fate decisions and transcriptional states and identify novel cell subpopulations through single-cell analysis. For example, Diether Lambrechts et al. performed an in-depth analysis of microenvironmental cells in lung cancer [17], and Nayoung Kim et al. investigated the microenvironment of metastatic LUAD [18]. Therefore, single-cell technology can be applied to study the types of ECs contained in the LUAD microenvironment, helping to reveal changes in function and impacts on prognosis to deepen the understanding of the role of stromal cells in the tumour microenvironment. However, it is not possible to study all endothelial cells based on current techniques. Therefore, it is very important to choose the right research object. The newly formed blood vessels in tumours have their own unique structural characteristics, as the tube wall is incomplete, without smooth muscle components, and composed of only porous endothelial cells and lamellar basal membranes. Studies have shown that these proteins play complex roles in the tumour microenvironment [19,20]. Most of the existing studies have focused on pathway research and drug targeting design as a whole; however, which cells in this large group exhibit functional changes in the microenvironment and the relationship of these changes with prognosis have not been elucidated. Recently, two homologous and differentiated capillary cell types were identified based on the identification of ECs in lung tissue by Jonas C. Schupp et al. [21] and the results of the specialized phenotype of vascular ECs by Astrid Gillich et al. [22]. These two types of cells are present mainly in the alveoli of normal lung tissue and perform their established functions. Whether the functions of these two kinds of cells change after the tissue becomes cancerous, as well as the influence of these changes on LUAD, must be further discussed (Fig. 1).

In this study, we obtained EC data for tumour tissue and paracancerous tissue after preliminary screening of existing single-cell data. Two homologous and differentiated capillary cell types were identified based on the marker genes identified in previous studies (FCN3, EDNRB, HPGD, PDPN, COL15A1, VWA1, ACKR1, SOX17, and GJA5) [23]. Some of these genes not only are marker genes but are also inextricably related to lung cancer. Among them, FCN3 plays an inhibitory role in LUAD by inducing endoplasmic reticulum stress [24]. EDNRB is a potential prognostic marker for patients with LUAD, and it may exert its function by modulating the ERK pathway in LUAD patients [25]. Cancer-associated fibroblasts expressing PDPN guide and enhance the local invasion of LUAD cells [26]. Reexpression of SOX17 in a lung cancer cell line inhibited Wnt signaling22. However, the direct relationships between lung cancer and HPGD, COL15A1, VWA1 and GJA5 have not been determined. The functional changes in the two kinds of capillary cells in tumour tissue and adjacent tissues, as well as interactions with other cells in tumour tissue and some genes that have characteristic expression patterns, were subsequently examined. The expression of these genes was combined with clinical and gene expression data for LUAD patients in the TCGA and GEO cohorts to analyse the correlation with prognosis, and the reliability of the results was verified by using multiple R packages. Prognostic models and risk scores were also used to group patients to analyse differences in clinical

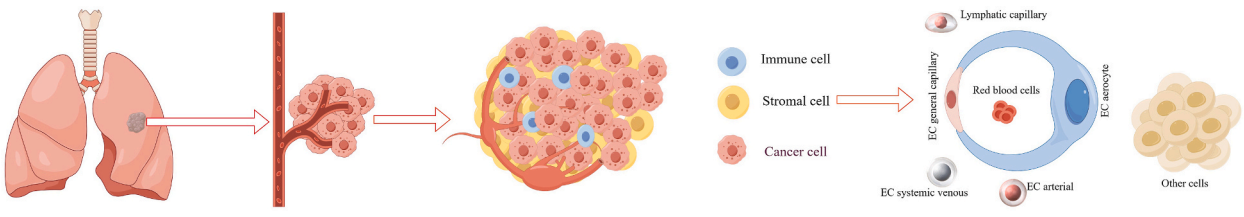

Fig. 1. ECs in the tumor microenvironment (By Figdraw).

characteristics, immune infiltration, and drug therapy efficacy and to evaluate clinical practicability.

2. Methods

2.1. Data collection and processing

Single-cell data were obtained from the GSE183219 dataset. For this dataset, ECs and immune cells were removed based on EpCAM and CD45 expression, respectively. CD29, which is present on all stromal cells, was used to enrich cells with intact surface markers. Sample preparation, processing and library construction of single cells were carried out in accordance with standard procedures.

2.2. Single-cell sample evaluation and clustering

Based on the GSE183219 data, 12 LUAD samples and 12 paracancerous tissue samples were extracted. For the tumour samples, quality control was carried out for each sample with the following criteria: subset = nFeature_RNA >200 & nFeature_RNA <5000 & percent.mt < 20 & nCount_RNA <100000, min.cells = 3, min.features = 200, and the FindVariableFeatures function set to the standard value. The FindIntegrationAnchors function was used to find and integrate the anchor points of the samples. The amount of

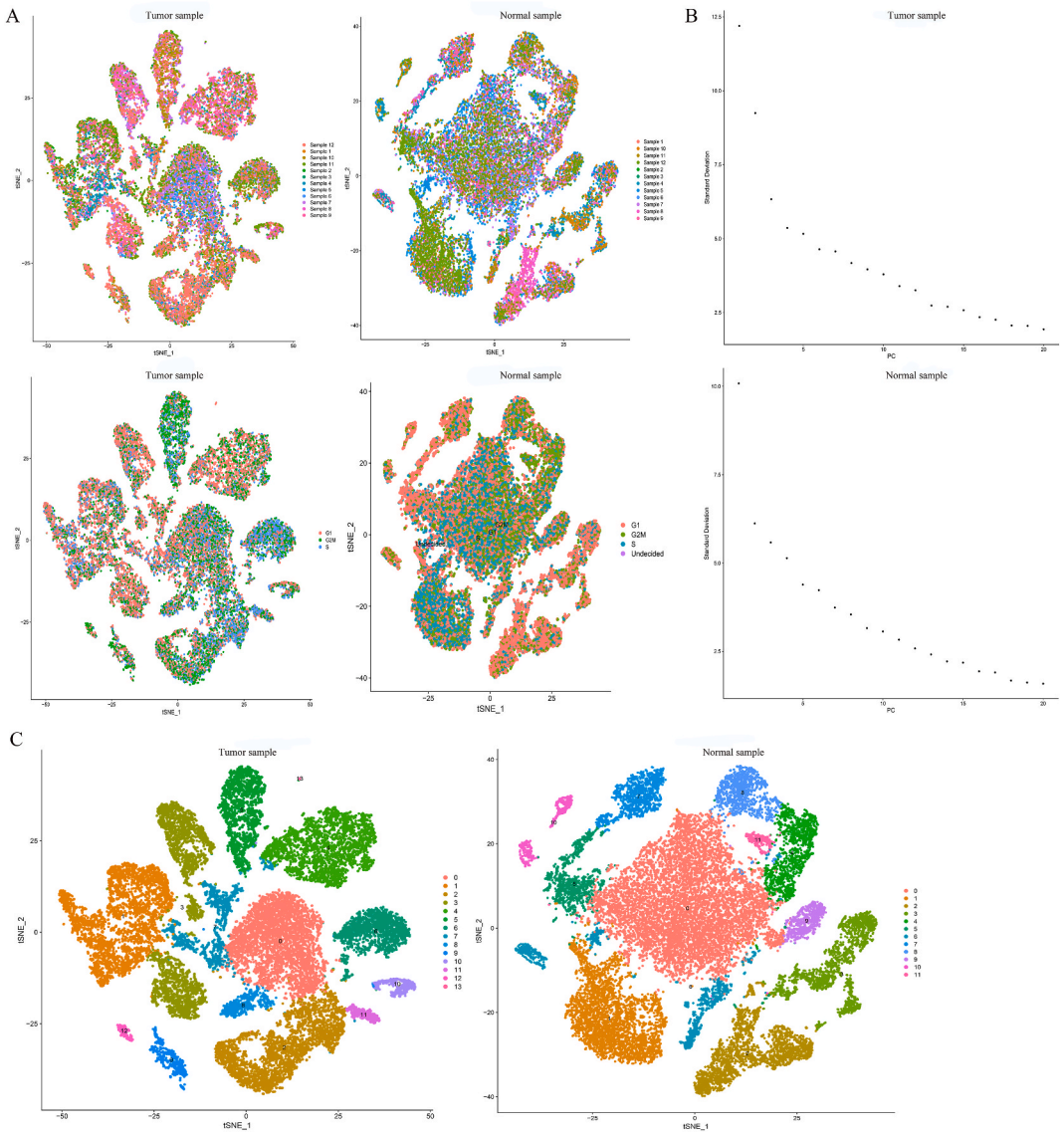

Fig. 2. Dimensionality reduction and cluster analysis of samples. Distribution of samples and cell stages in two tissue types (A). The selection range of principal components (PCs) (B). Cluster number of single-cell data in tumour tissue and normal lung tissue (C).

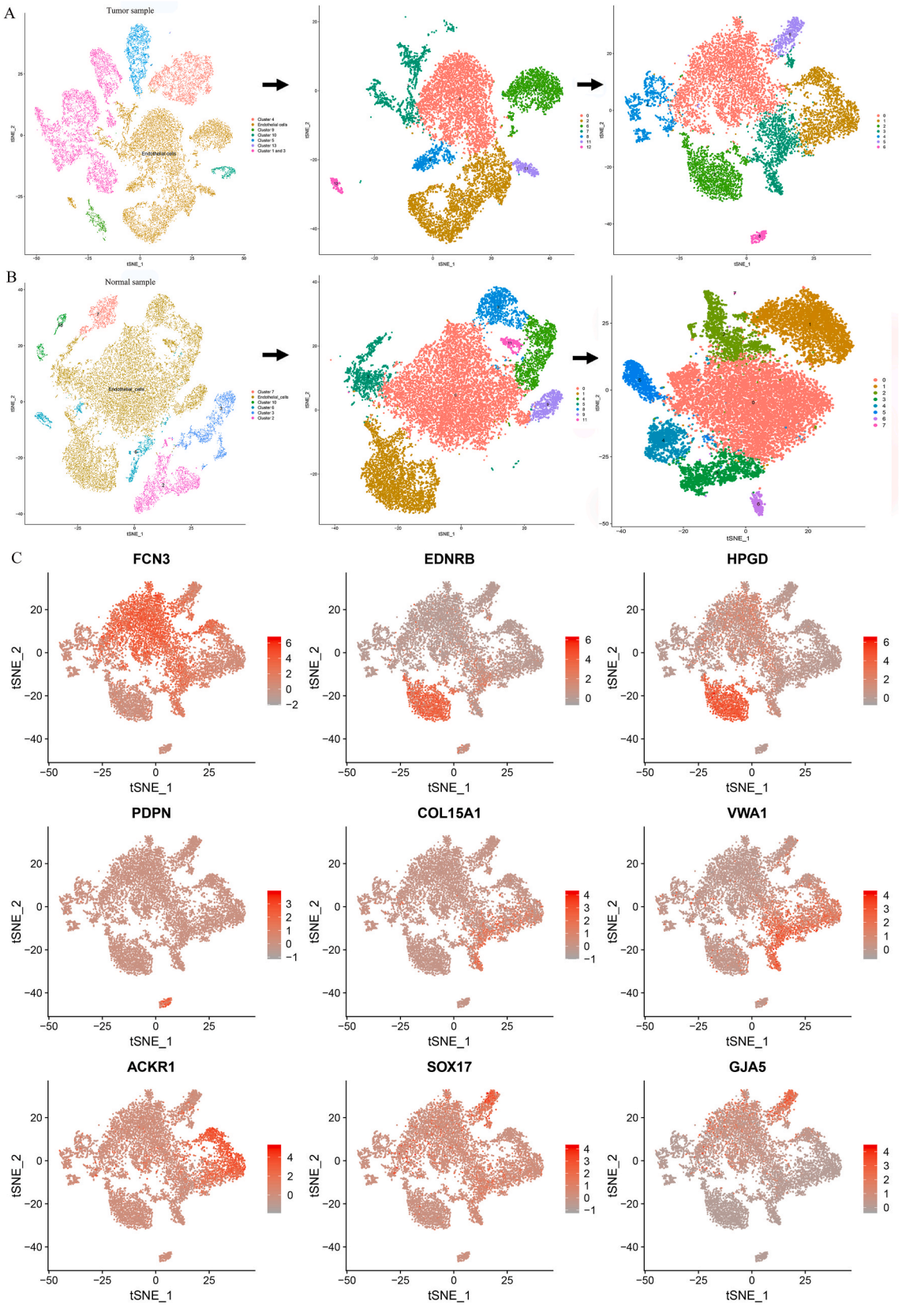

(caption on next page)

Fig. 3. Extraction and recognition of ECs in the microenvironment. Extraction and reclustering of ECs from the tumour tissue microenvironment (A) and normal lung tissue microenvironment (B). Expression of marker genes in reclustering of ECs in the tumour microenvironment (C).

data to be analysed for a single cell is very large and high-dimensional, involving tens of thousands of cells, which are difficult to distinguish during direct analysis; therefore, these high-dimensional data need to be reduced, and feature selection needs to be performed. After linear dimensionality reduction through Principal component analysis (PCA), nonlinear dimensionality reduction of t-distributed stochastic neighbour embedding (t-SNE) was carried out, and similar cells were clustered after appropriate values of "dims" and "resolution" were selected. The information about cell clusters can be better represented by images. This is done through the FindIntegrationAnchors, RunPCA and RunTSNE functions in the Seurat package [27]. The distribution of cells in the samples and the dimensionality reduction of the cell cycle were subsequently investigated to determine any potential influence on cell classification. The same procedure was performed for paracancerous tissue samples.

2.3. Cell annotation, subpopulation extraction and functional pathway analysis

The functionality of the SingleR package [28] was used in R to annotate the clusters of cells in consolidated data and extract cell subsets annotated as ECs. Then, appropriate values of "dims" and "resolution" were set to recluster the extracted subpopulations, and the cluster was further annotated in combination with cell marker genes verified in the literature. Lymphatic ECs were identified on the basis of the expression of the canonical lymphatic marker PDPN. Arterial ECs were identified by SOX17 and GJA5. Systemic venous ECs were identified by ACKR1, COL15A1 and vWA1 expression. EC aerocytes were identified by EDNRB and HPGD. The EC general capillaries were identified by FCN3 [21]. Functional pathway analysis was carried out through the Gene Set Variation Analysis (GSVA) program package [29] to assess the functional changes between tumour samples and normal samples. The Seurat, ggrepel [30], and ggplot2 [31] packages were used to map DEGs in different types of ECs.

2.4. Cell communication analysis and expanded sample analysis of endothelial cells

The CellPhoneDB function module in Python was downloaded, and the cell-to-cell communication relationships between the tumour samples and adjacent tissue samples were analysed [32]. In the obtained expression matrix and cell annotation, for the

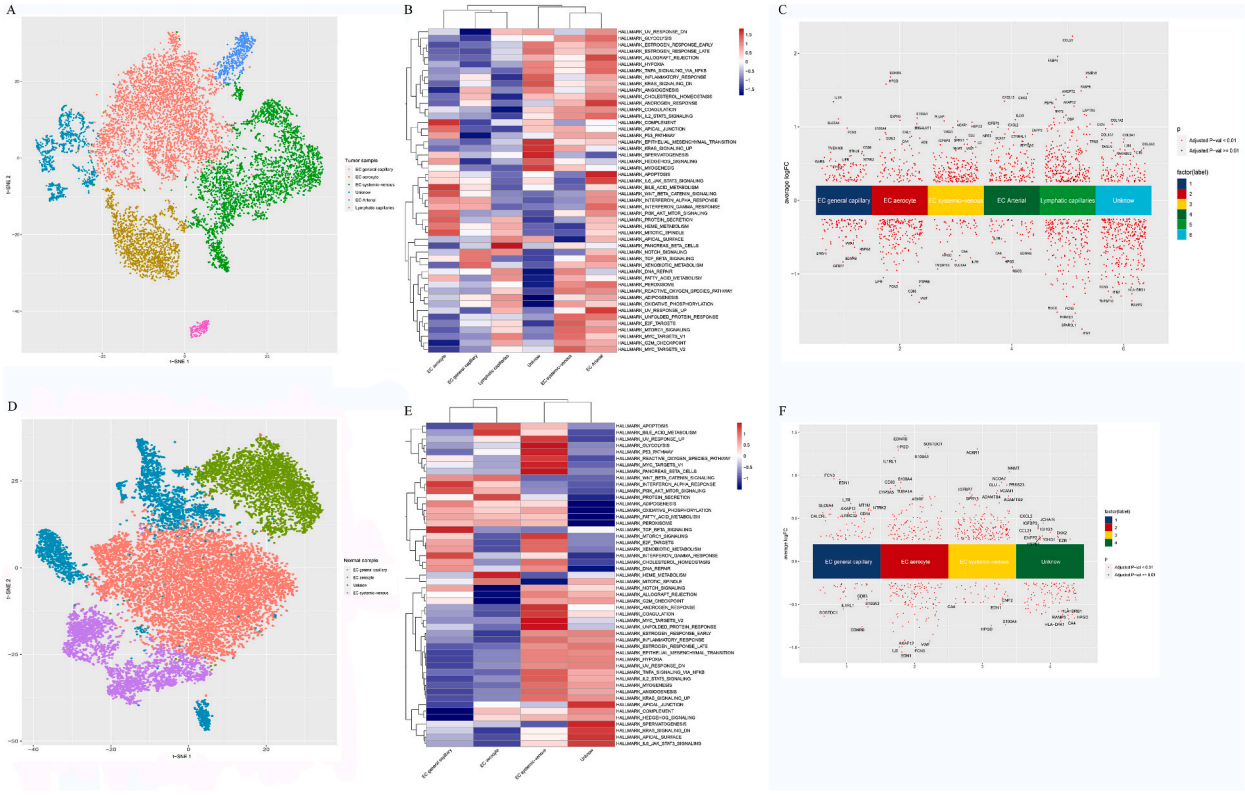

Fig. 4. Identification and functional annotation of ECs. Types of ECs (A), annotations of the top 50 functional pathways (B), and differential marker genes for each EC in tumour samples (C). Types of ECs (D), annotations of the top 50 functional pathways (E), and differential marker genes for each EC in normal samples (F).

interaction of Gene1-Gene2, the expression MEAN of gene1 in "clusterA" and of gene2 in "clusterB" were calculated, and the mean of the two was used as the mean. After the labels of the cells were randomly changed, the mean expression of gene1 in "clusterA" and gene2 in "clusterB" was calculated according to the new label, and the average mean was subsequently obtained. After this process is repeated many times, a mean distribution can be obtained. The position of the MANs in this distribution and the more extreme positions constitute a fraction of the p value (the definition of a p value). Therefore, CellPhoneDB speculates that the significant enrichment of ligands between two cell types is essentially based on the amount of receptor expression in one cell type and the amount of ligand expression in the other cell type. Subsequently, the "ktplots" package [33] was used in R for a visual graphical display of the generated result file. The gene features of the ECs identified in the tumour samples and normal samples were mapped to TCGA data to obtain the levels of both EC aerocytes and EC general capillary cells and to analyse the prognostic correlation (CIBERSORT website and R). The annotated EC aerocyte and EC general capillary subgroups were extracted from the tumour samples to identify genes differentially expressed between the two populations and to classify them as upregulated or downregulated (genes with pval adj >0.05 were removed). Similarly, this type of data analysis was performed for paracancerous tissues. The genes were classified, and a Venn diagram was created to visualize changes unique to the tumour samples.

2.5. Mutation information and clustering grouping of differentially expressed genes

Gene mutation information, expression matrix data and clinical feature data of LUAD patients were downloaded from the TCGA database to examine mutations in the differentially expressed genes in TCGA LUAD patients obtained by the above procedure. The gene expression matrix and clinical features of LUAD patients were downloaded from the GSE68465 and GSE11969 datasets and integrated with the TCGA data. Univariate Cox analysis was used to further screen out genes associated with prognosis among the differential genes; the correlation of these genes was analysed, and patients with pulmonary glands were grouped based on these genes.

2.6. Characteristic differences between the types

The difference in survival between subtypes was analysed with clinical data. Because some of the clinical data in the GEO cohort could not be matched with the data in the TCGA cohort, only the information in the TCGA cohort was used to determine differences in the characteristics of clinical patients among different subtypes and to determine differences in the expression of differentially expressed genes among subtypes.

2.7. Construction and evaluation of the prognostic model

First, the reliability of the classification was checked by PCA dimensionality reduction. R was subsequently used to identify genes differentially expressed between different subtypes (parameter set as logFCfilter = 1, adj.p.Val.filter = 0.01). Univariate Cox analysis was performed for the DEGs, followed by least absolute shrinkage and selection operator (LASSO) regression analysis to screen for suitable genes for the construction of prognostic models. These genes were searched in the UALCAN database and the differential expression maps between tumor samples and normal samples were downloaded. The model calculation formula was as follows: βgene1 × expressiongene1 + βgene2 × expressiongene2 + βgene3 × expressiongene3 + … + βgenen × expressiongenen, where β

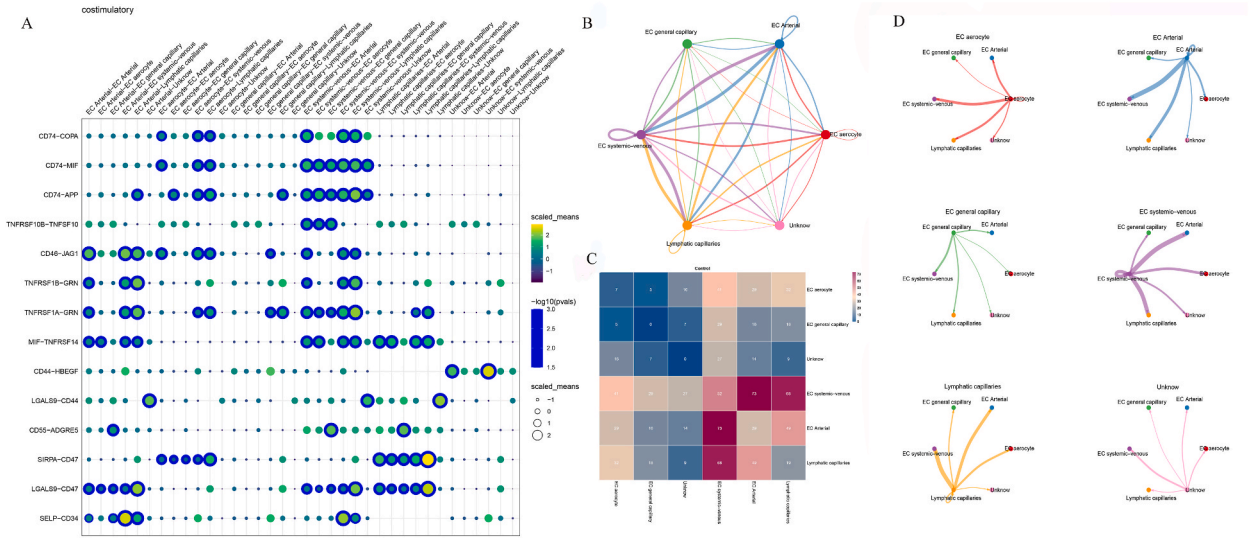

Fig. 5. CellPhoneDB results of ECs in the tumour sample. The degree of association of costimulatory molecules between various endothelial cells (A). Intensity of interactions between various endothelial cells (B, D) and quantified heatmaps (C).

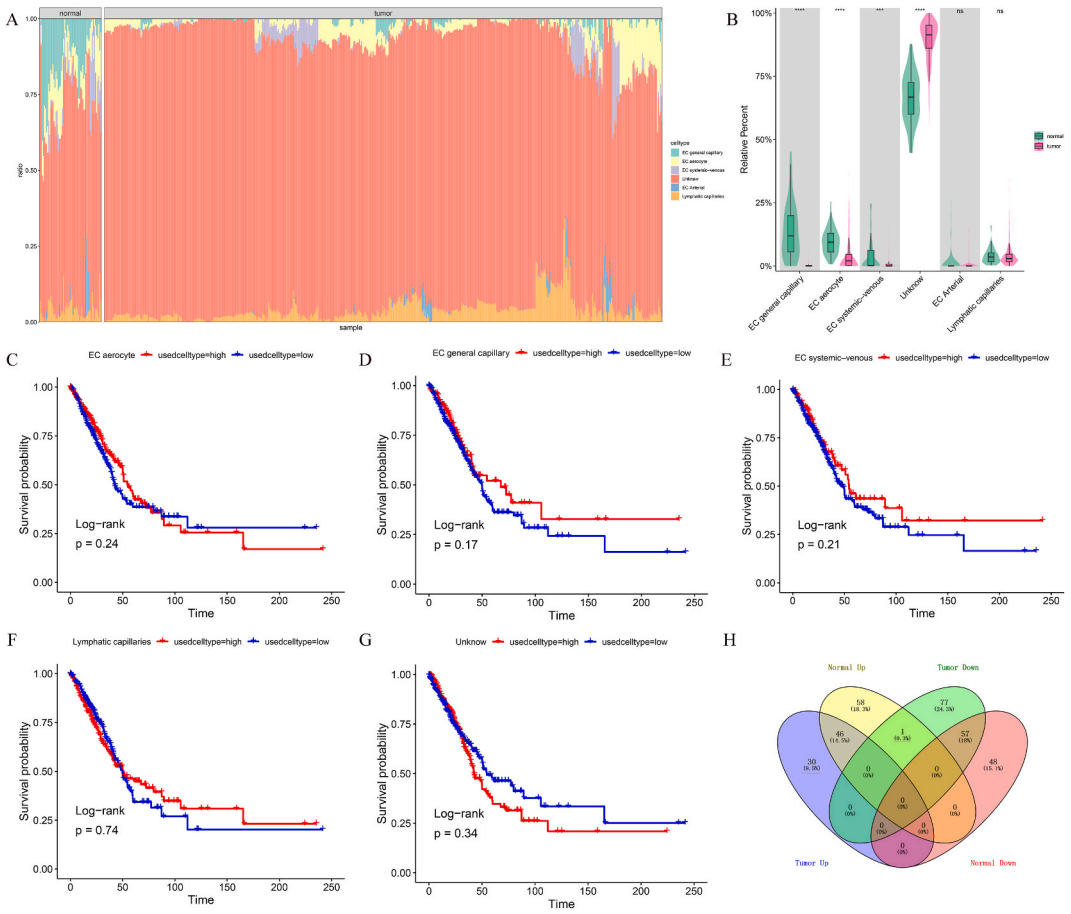

Fig. 6. Sample expansion analysis and differential gene change analysis of ECs. The content distribution (A) and difference (B) of various ECs in tumour samples and normal samples. EC aerocyte (C), EC general capillary (D), EC systemic - venous (E), lymphatic capillary (F) and unknown EC (G) content differences and the survival time curve. Changes in differentially expressed genes in two types of specialized capillary endothelial cells (H).

refers to the coefficient value in the multivariate Cox analysis and Expressiongene refers to the expression level of a gene in patients with LUAD. The patients were subsequently divided into a high-risk group and a low-risk group according to the median risk score. The combined TCGA and GEO data were grouped using a prognostic model to examine differences in risk scores among subtypes and to verify differences in survival and expression of differentially expressed genes between high- and low-risk groups. The patients were divided into a training group and a test group. A receiver operating characteristic (ROC) curve was drawn based on the prognostic model, and the accuracy of the area under the ROC curve (AUC) was calculated and compared with that of the existing prognostic model. Next, a nomogram was constructed to integrate clinicopathological features with risk groups to verify the accuracy of the prognostic prediction. A receiver operating characteristic (ROC) curve was also plotted, and the area under the curve (AUC) was calculated.

2.8. Relationships of prognostic models with immune cells and drug therapy efficacy

The Spearman correlation was used to analyse the correlation between genes in the model and immune cells, as well as the correlation between the risk scores of the samples calculated based on these genes and immune cells and stem cells (CIBERSORT in R) [34]. The pRRophetic package [35] was used to calculate the relationship between the half-maximal drug inhibitory concentration (IC50) of different drugs commonly used in pulmonary glands and the risk score.

2.9. Statistical analysis

Statistical analysis and visualization were performed using R (version 4.2.2) and the corresponding R packages. Kaplan-Meier survival curves were generated, and univariate and multivariate Cox regression analyses were performed using the "Survival" R package. Chi-square tests or Fisher precision tests were used to compare differences in clinical features between the two risk groups.

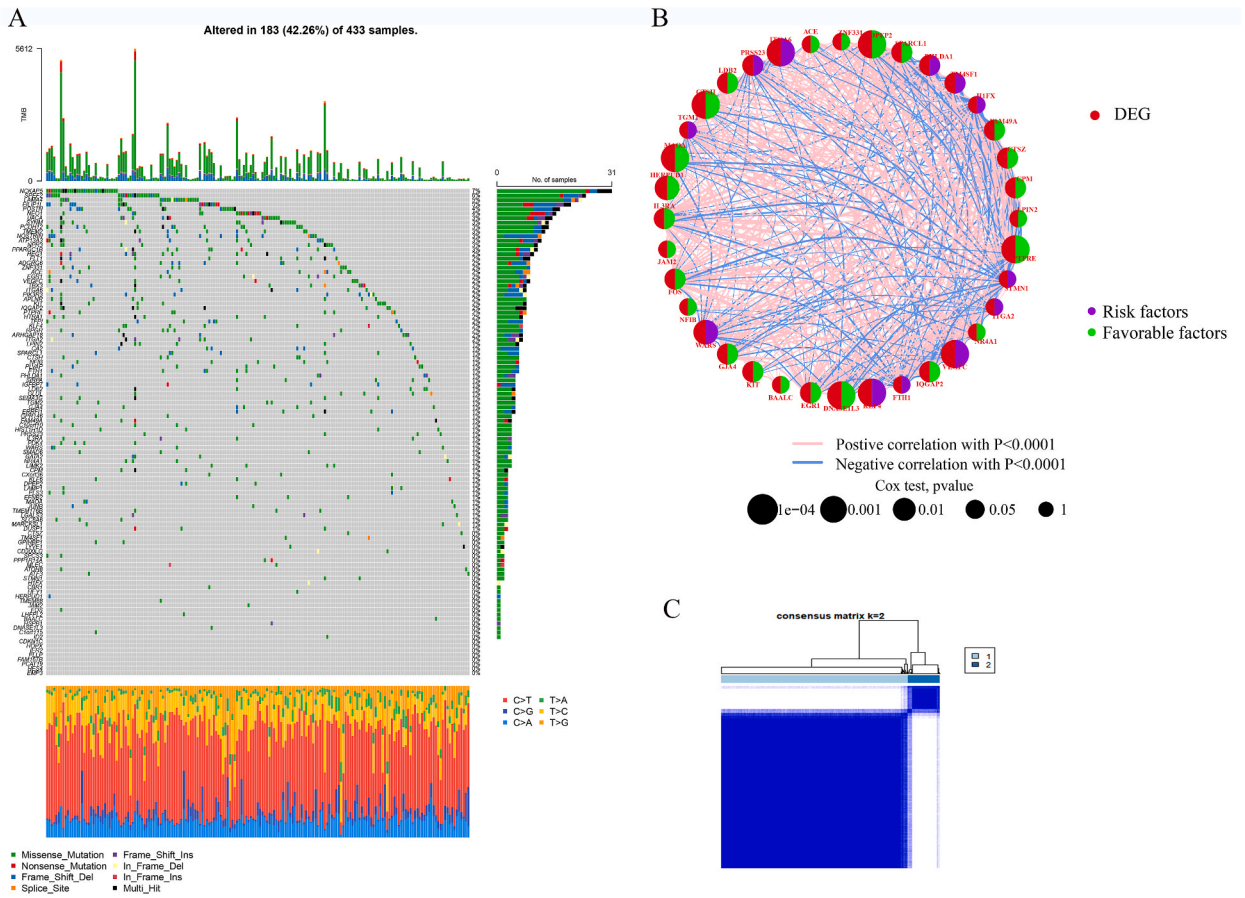

Fig. 7. In-depth analysis of differentially expressed genes in TCGA. Display of mutation information for 108 genes (A). Correlation between prognostic differential genes, where purple represents prognostic correlation and green represents positive prognostic correlation (B). Prognostic differential genes divided the LUAD patients in TCGA into two groups (C). (For interpretation of the references to colour in this figure legend, the reader is referred to the Web version of this article.)

The Wilcoxon rank sum test was used to compare differences in continuous variables. Spearman correlation analysis was used to evaluate the correlation between the expression of the model genes and the number of infiltrating immune cells. Gene coexpression analysis was calculated by Pearson correlation analysis. If not otherwise indicated, a P value < 0.05 was considered to indicate statistical significance.

3. Results

3.1. Characteristic distribution of samples and annotated results of cells

A quality control diagram of the tumour samples and adjacent normal lung tissue samples is shown in Supplementary Material 1. Fourteen cell subpopulations were obtained from the tumour samples (parameter set to PCA 20, resolution 0.2; Supplementary Material 2A), and twelve cell subsets were obtained from the adjacent normal lung tissue samples (parameter set to PCA 20, resolution 0.2; Supplementary Material 2B) (Fig. 2B and C). The distribution and cell cycle distribution of the tumour samples and adjacent normal lung tissue samples are shown in Fig. 2A. ECs from the two types of tissues were screened by singR annotation screening in R (Fig. 3A and B), extracted and regrouped. A total of 7 clusters were obtained for the tumour samples, and 8 were obtained for the adjacent normal lung tissue samples (parameter set to dims 1:20, resolution 0.2 in FindNeighbors). (Supplementary Material 3). Combined with previously published research, the identified EC marker genes were used to distinguish clusters in the tumour (Fig. 3C) and adjacent normal lung tissue (Supplementary Material 4) samples.

3.2. Functional information of different types of EC

The cell subpopulations were further annotated by marker genes (Fig. 4A and D). In the tumour samples, we identified the EC general capillary, EC aerocyte, EC systemic venous, EC arterial, and lymphatic capillary subtypes, although some clusters could not be

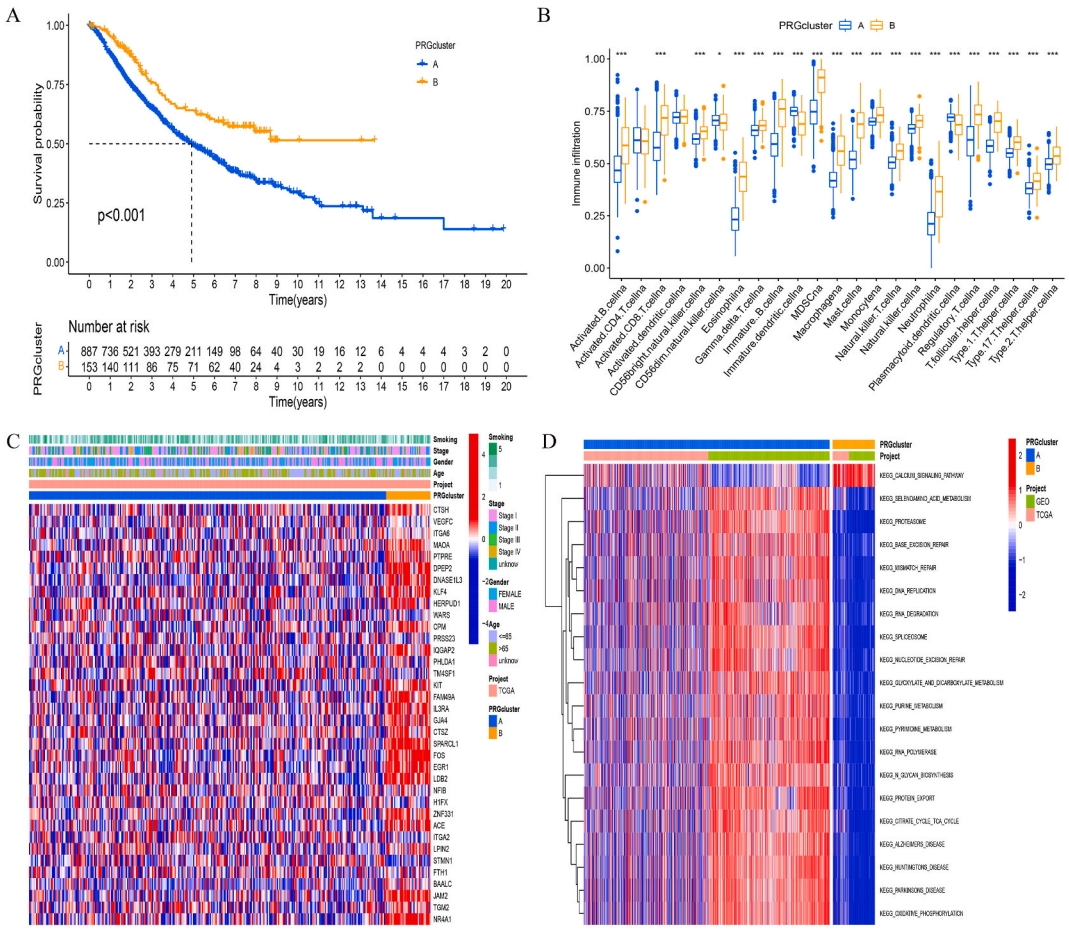

Fig. 8. Characteristic differences between the two groups. Significant difference in prognosis between the two groups (A). Significant differences in immune cell infiltration between the two groups (B). Clinicopathological features and gene expression between the two groups (C). The KEGG pathway distribution was different between the two groups (D).

identified. We identified the EC general capillary, EC aerocyte, and EC systemic venous subtypes in the paracancerous tissue samples, as well as some unidentifiable clusters. These subpopulations were functionally annotated to assess the difference in function between the same type of EC subpopulation in tumour samples and adjacent tissue samples (Fig. 4B and E). The signature genes of these cells are shown, and the top 10 genes are labelled in Fig. 4C and F.

3.3. EC communication, ECs and differential gene screening in LUAD samples

The relationships of costimulatory molecules with the six types of ECs were determined via CellPhoneDB analysis (Fig. 5A); moreover, the interactions between various ECs were also determined (Fig. 5B and D). The number of interactions between different ECs was quantified, and a heatmap was drawn (Fig. 5C). By combining the specific genetic characteristics of various ECs with TCGA gene expression data, we obtained the proportions and differences between tumour samples and normal samples (Fig. 6A and B). However, subsequent survival data analysis failed to reveal a correlation between the EC concentration and survival prognosis, but differences in the content of EC general capillaries and EC aerocytes were found in LUAD patients at different time points (Fig. 6C–G). Based on the homologous characteristics of the two types of cells as the research background, subsequent differential gene analysis was conducted to determine the changes in the DEGs between the tumour tissue and normal lung tissue. The genes differentially expressed between the EC general capillary and EC aerocyte subtypes in tumour tissue samples and paracancerous tissues were extracted (Supplementary Material 5). The extracted genes were divided into upregulated genes and downregulated genes and intersected (Fig. 6H) to obtain 108 genes with differential expression in tumour tissues versus adjacent tissues.

3.4. Expression of differentially expressed genes in the databases

Mutation information for the selected genes was displayed using TMB data from the downloaded TCGA database (Fig. 7A). Using the TCGA, GSE68465 and GSE11969 datasets, 108 genes were preliminarily subjected to univariate Cox analysis, and 36 genes related

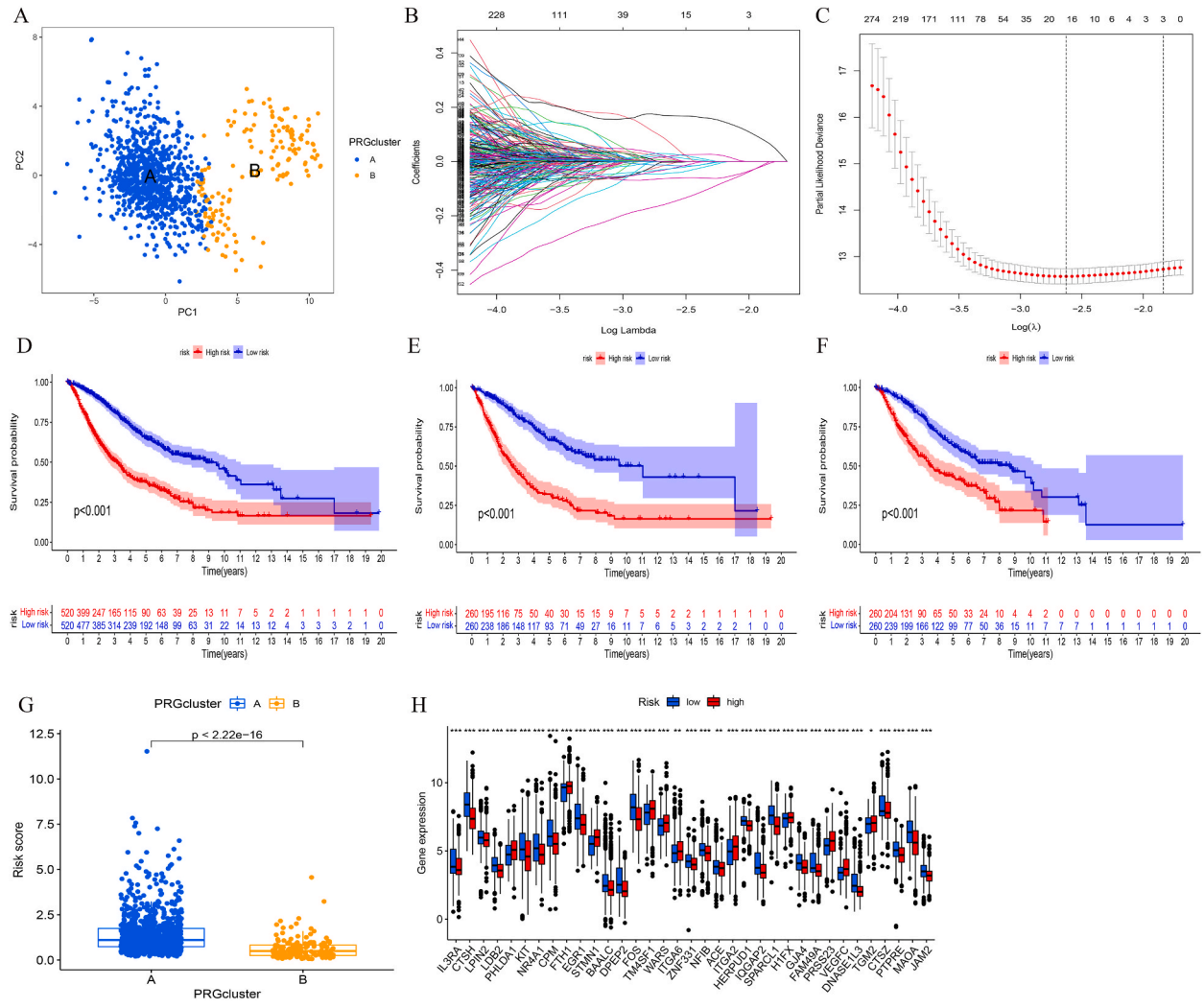

Fig. 9. The division of risk groups and the relationship between risk groups and cluster groups. Dimension reduction analysis between cluster groups (A). LASSO regression analysis of different genes between groups (B, C). Significant prognostic differences between risk groups in the total data (D), training set (E) and test set (F). Obvious differences in risk scores among cluster groups (G). Differential expression of genes among risk groups (H).

Table 1
Multivariate Cox proportional hazards regression analysis.

Gene	coefficient value
NDRG1	0.17014
GSTA3	−0.22152
NPAS1	0.32838
FAIM2	−0.14953
CHEK1	0.28621
ABAT	−0.34306
CD19	−0.14815
PTPRCAP	−0.08262

to prognosis were screened out. In addition, risk and favourable genes among these genes, as well as their correlation properties, including positive and negative correlations, were obtained through a drawn circle diagram (Fig. 7B). These genes were subsequently used to classify LUAD patients into two groups (Fig. 7C).

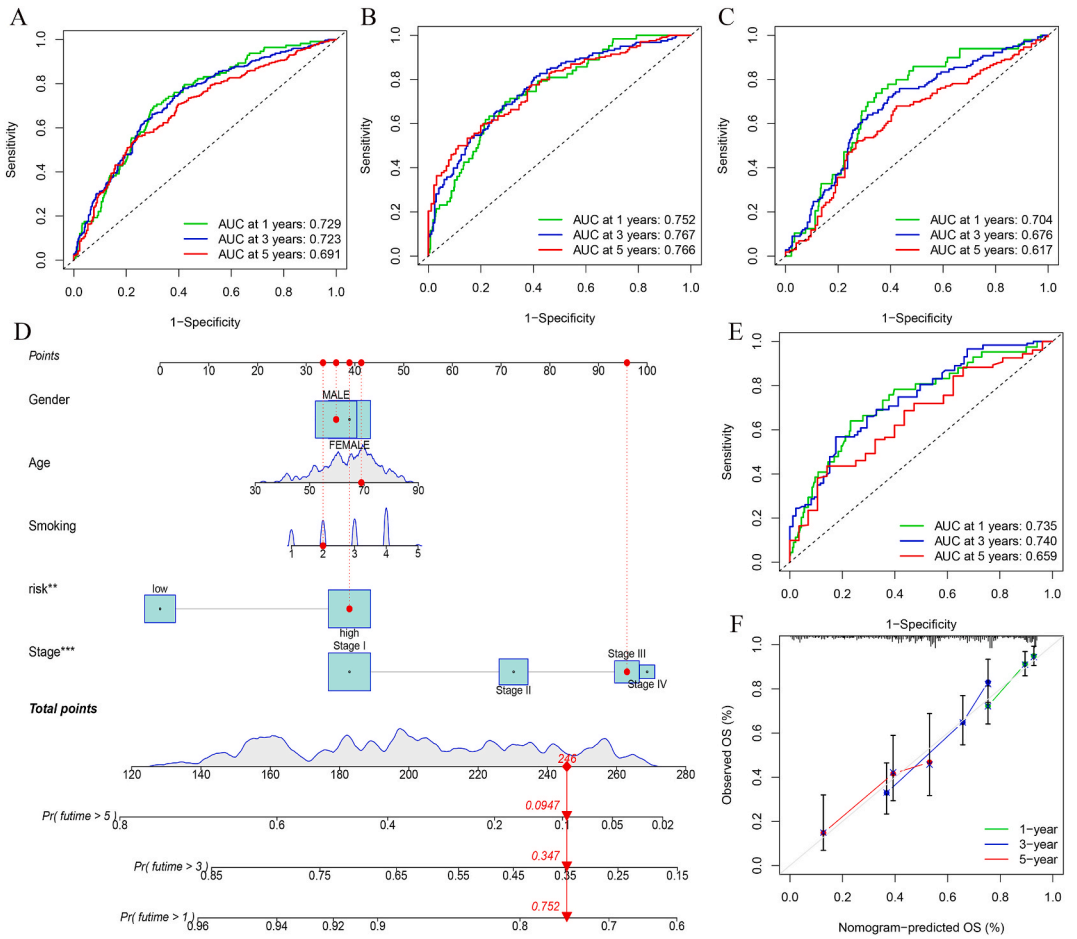

Fig. 10. Performance prediction of the prognostic model and construction of the nomogram. Prognostic model AUC values for survival at 1, 3, and 5 years in the total dataset (A), training set (B) and test set (C). The constructed nomogram (D), its AUC values for survival at 1, 3, and 5 years (E) and validation results (F).

3.5. Differences in clinical features between tumour subtypes

As described above, LUAD patients were defined as type A or type B, and analysis of prognostic expression data revealed prognostic differences between the two types of LUAD ($P < 0.001$) (Fig. 8A). By using the single-sample gene set enrichment analysis (ssGSEA) calculation score on the sample integration data from the TCGA and GEO cohorts, differences in immune infiltration between type A and type B patients were found (Fig. 8B). By comparing the clinicopathological feature data (smoking status, stage, sex, age) of the two subtypes, as well as the expression of the above 36 genes, it can be concluded that there are obvious differences in these features between the two subtypes (Fig. 8C). Smoking history was defined as follows: a lifelong nonsmoker (<100 cigarettes smoked in lifetime) = 1, current smoker (including daily smokers and nondaily smokers or occasional smokers) = 2, current reformed smoker for >15 years = 3, current reformed smoker for ≤15 years = 4, current reformed smoker, duration not specified = 5). Because the TCGA data could not be synchronized with the GEO data, only relatively comprehensive TCGA data were used. GSVA revealed significant differences in the Kyoto Encyclopedia of Genes and Genomes (KEGG) pathways between the two groups of patients, with the "CALCIUM SIGNALING PATHWAY" exhibiting significantly greater enrichment in the B type and the opposite occurring for the other pathways (Fig. 8D).

3.6. Applicability and accuracy of the prognostic model

By dimensionality reduction of the A and B classification data, the degree of dispersion was shown to be appropriate, indicating that the classification was accurate (Fig. 9A). After LASSO regression analysis (Fig. 9B and C), suitable and reliable genes were selected for construction of a prognostic model consisting of eight genes (ABAT, CD19, CHEK1, FAIM2, GSTA3, NDRG1, NPAS1, and PTPRCAP) obtained by proportional risk regression analysis (Table 1). Differential expression maps for these genes in Supplementary Material 6. Risk score = (0.17014 × expression of NDRG1) + (−0.22152 × expression of GSTA3) + (0.32838 × expression of NPAS1) +

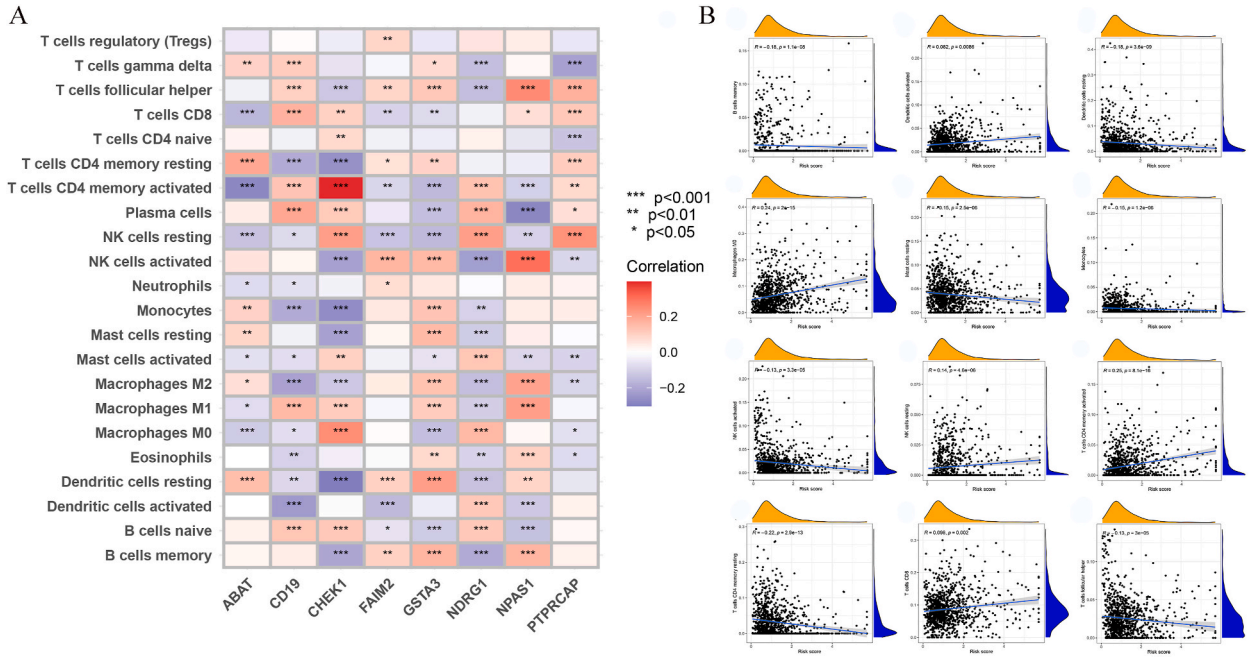

Fig. 11. Combined analysis of the prognostic model and immune infiltrating cells. The relationship between genes and immune cells in the construction of the prognostic model (A). Relationship between risk grouping and immune cells (B).

(−0.14953 × expression of FAIM2) + (0.28621 × expression of CHEK1) + (−0.34306 × expression of ABAT) + (−0.14815 × expression of CD19) + (−0.08262 × expression of PTPRCAP). The patients were divided into risk groups based on the prognostic model, and the survival time between the high-risk and low-risk groups significantly differed (Fig. 9D). The data were also divided into training and test sets, and the difference in prognosis between the high-risk and low-risk groups was also evaluated (Fig. 9E and F). The difference in risk scores between the type A and B groups is depicted in Fig. 9G. Among the 36 genes involved, 35 exhibited differences in expression between the high- and low-risk groups (Fig. 9H), although the difference in KLF4 expression was not statistically significant. According to the prognostic model, the area under the curve (AUC) for survival at 1, 3, and 5 years was 0.729, 0.723, and 0691, respectively (Fig. 10A), with better survival in the training cohort (0.752, 0.767, and 0.766, respectively) (Fig. 10B) and slightly worse survival in the test cohort (0.704, 0.676, and 0.617, respectively) (Fig. 10C). Comparisons with other models are shown in Supplementary Material 7. Clinicopathological features were combined with the risk score to construct a nomogram (Fig. 10D), and the prediction of survival at 1, 3, and 5 years matched the real survival time, as illustrated in Fig. 10F; the area under the curve (AUC) for survival at 1, 3 and 5 years was 0.735, 0.740 and 0.659, respectively. The data used herein are only clinically relevant from the TCGA cohort (Fig. 10E). The reason is that the available data on clinicopathological features in the GEO cohort are not comprehensive enough.

3.7. Immunological correlation and drug treatment differences

The CIBERSORT results showed that the 8 genes composing the prognostic model had different associations with cells involved in the immune response; among these genes, CHEK1 had the strongest correlation with activated memory $CD4^+$ T cells, and FAIM2 had the weakest correlation with immune cells. However, FAIM2 was the only gene associated with regulatory T cells (Tregs) (Fig. 11A). The risk score calculated by the model correlated positively with activated dendritic cells, M0 macrophages, resting NK cells, activated memory $CD4^+$ T cells, and $CD8^+$ T cells. In contrast, the proportions of memory B cells, resting dendritic cells, resting mast cells, monocytes, activated NK cells, resting memory $CD4^+$ T cells, and follicular helper T cells were negatively correlated (Fig. 11B). The number of tumour stem cells also correlated positively with the risk score (Fig. 12A). Compared with those in the high-risk group, the low-risk group exhibited good sensitivity to cisplatin, docetaxel, gemcitabine, paclitaxel, etoposide, and vinorelbine and poor sensitivity to axitinib, ABT-888, and ATRA (Fig. 12B–J).

4. Discussion

Here, we present a detailed map of ECs in the LUAD microenvironment. We optimized marker genes of different ECs based on the results of previous studies. By elucidating the relationships between differences in vascular EC differentiation and the occurrence and development of LUAD, we have provided a better understanding regarding the importance of the stromal microenvironment in tumour research. By establishing these effects in the form of differences in clinical data, reasonable research directions can be explored.

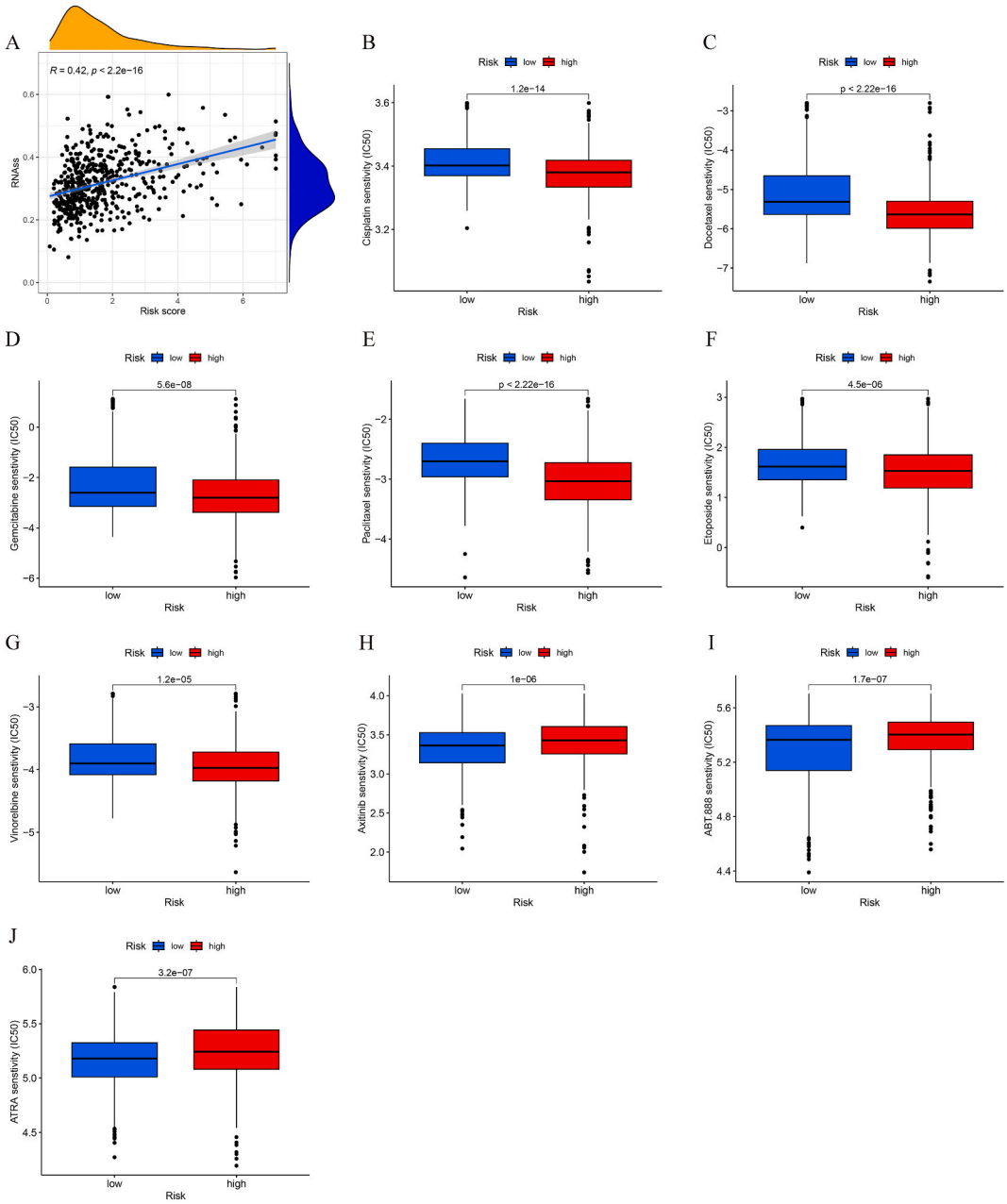

Fig. 12. Significance of the risk score and risk grouping in clinical treatment. A positive correlation between the risk score and tumour stem cell index (A). A significant difference between the low- and high-risk groups was found for cisplatin (B), docetaxel (C), gemcitabine (D), paclitaxel (E), etoposide (F), vinorelbine (G), axitinib (H), ABT.888 (I), and ATRA (J).

There are many kinds of cells, and under comprehensive analysis of the existing data, these cells can be identified and classified only to a certain extent. The role of different capillary differentiation types in the LUAD microenvironment, as well as their prognosis and efficacy, are the focus of our research. After analysing the existing data, we identified five types of ECs in the microenvironment in tumour samples and three types of ECs in normal lung tissue samples based on the expression of marker genes. Among these different types of ECs, we found that the EC general capillary, EC aerocyte, and EC systemic venous subtypes can be well distinguished in the two different tissues. The EC general capillary and EC aerocyte subtypes are derived from bipotent progenitors. The EC general capillary subtype functions in the lung to regulate vasomotor tension; as stem/progenitor cells in capillary homeostasis and repair, EC aerocytes perform gas exchange and transfer of white blood cells [22]. Both types of specialized capillary ECs play important roles in the lung.

The growth of tumours occurs through the formation of new blood vessels to provide nutrients for their growth, promoting the metastasis and spread of tumour cells far from the primary site [36,37]. During tumour progression, blood vessels develop from

existing capillaries or postcapillary veins [38–40]. The processes involved include activation of ECs, degradation of the basement membrane and extracellular matrix, migration and proliferation of ECs, formation of blood vessels and extension of blood vessels into solid tumours. It is obvious that the functional activities of ECs play an important role. The EC general capillary and EC aerocyte subsets are different differentiation phenotypes of capillary ECs. They perform specific functions in normal lung tissue, and we found many functional changes in these tissues. As shown in Fig. 4, these differences involved mainly the HallMark complement, HallMark apical junction, HallMark p53 pathway, HallMark complement, HallMark apical junction, HallMark p53 pathway, HallMark mtorc1 signalling, HallMark E2F targets, HallMark DNA repair and HallMark oxidative phosphorylation pathways. These pathways are inextricably linked to tumour growth. The complement system is an often overlooked component of the tumour microenvironment [41]. Previous studies have shown that malignant cells and infiltrating cells can produce a large amount of complement protein [42], thereby participating in different tumour growth activities. Endothelial and epithelial cells constitute the body's osmotic barrier with apical junctions [43–45]. In gastric cancer, scoring apical junction function can predict patient survival, possibly due to increased metastatic potential through EMT and angiogenesis [46]. The relationship between the p53 pathway and tumours has been confirmed by various scholars [47,48], and it is closely related to tumour vascular growth [49,50]. Mtorc1 signalling is one of the pathways that promotes cell growth, and its dysregulation can lead to abnormal growth of blood vessels [51].

According to our cell communication analysis, there is a close relationship between ECs. Although tumour cells could not be well identified for joint analysis, the results of this and previous studies allowed us to preliminarily conclude that tumour cells have a certain degree of influence on ECs. These functional changes in ECs may vary according to type; for example, they may not be able to perform their normal functions, resulting in abnormal organ function, or they may have an intricate relationship with tumour angiogenesis. This study focused on two specialized types of capillary ECs that may be associated with tumour angiogenesis. Through supplementary analysis of TCGA data, it was found that in addition to functional changes, the proportions of these two kinds of cells significantly differed between tumour and normal tissue samples, but the difference in content had no statistically significant prognostic correlation. Nevertheless, the prognostic curve indicated that the difference in the proportions of these two kinds of cells during different periods may be related to the difference in survival time. The two kinds of cells are homologous, and the differential expression of genes between them may reflect a difference in differentiation. This study also revealed differences in the expression of these genes between tumour samples and normal tissue samples. Therefore, it can be preliminarily hypothesized that the differentiation of these two cell types may be influenced by other cells in the tumour microenvironment. We visualized these differences and obtained an 8-gene (ABAT, CD19, CHEK1, FAIM2, GSTA3, NDRG1, NPAS1, and PTPRCAP) prognostic model through comprehensive analysis of public databases. The prediction performance of this model was more accurate than that of a previous model [52–54]. Among these genes, the main function of 4-aminobutyrate aminotransferase (ABAT) is amino-butyl catabolism, and its reduced expression is associated with endocrine therapy resistance in breast cancer and progression of liver cancer [55,56]. CD19 is an immunoglobulin expressed by B lymphocytes that plays an important role in the activity of immune cells in the lung cancer microenvironment [57,58]. The purpose of CHEK1 is to identify DNA damage and nonreplication, which are closely related to the occurrence of non-small cell lung cancer and drug resistance [59]. FAIM2 is involved in the process of apoptosis and can promote non-small cell lung cancer cell growth and bone metastasis by activating the Wnt/β-catenin pathway [60]. GSTA3 acts as a cellular defence against toxic and carcinogenic substances, and its expression in alveolar cells induces an oxidative stress response [61]. The protein encoded by the NDRG1 gene is involved in the stress response, cell growth and differentiation and has been implicated in angiogenesis and drug resistance in lung cancer [62,63]. The function of the NPAS1 gene is still unclear, and deletion polymorphisms have been found only in breast cancer [64]. Although the role of PTPRCAP in lung cancer is unclear, studies have shown that certain polymorphisms are associated with susceptibility to and gene expression in diffuse gastric cancer [65]. These genes deserve further study and may serve as targets.

5. Conclusions

Finally, we summarized our findings and identified two main subtypes of capillary ECs in the lung adenocarcinoma microenvironment. These two specialized types of cells appear to undergo functional changes during tumour growth, which may be influenced by tumour cell activity. These functional changes are reflected by a series of gene function changes, and comprehensive analysis of these genes can be used to predict the prognosis of LUAD patients and drug efficacy. Whether changes in the function of these genes can normalize capillaries from tumour regression through drug therapy is worthy of further investigation.

Funding

This research received no external funding.

Data availability

The code is provided in the Supplementary code Material. Source data are provided with this paper. All other datasets generated and analysed in the current study are available from the corresponding author upon reasonable request.

Ethics declarations

Informed consent was not required for this study because the data comes from public database.

CRediT authorship contribution statement

Rongchang Zhao: Writing – review & editing, Writing – original draft, Visualization, Validation, Supervision, Software, Resources, Project administration, Methodology, Investigation, Formal analysis, Data curation, Conceptualization. **Yan Ding:** Investigation, Formal analysis, Data curation. **Rongbo Han:** Software, Methodology, Formal analysis. **Rongjie Ding:** Validation, Supervision, Software. **Jun Liu:** Supervision, Resources, Investigation. **Chunrong Zhu:** Visualization, Supervision, Software. **Dan Ding:** Writing – review & editing, Writing – original draft, Visualization, Validation. **Minhui Bao:** Writing – review & editing, Validation, Resources.

Declaration of competing interest

The authors declare that they have no known competing financial interests or personal relationships that could have appeared to influence the work reported in this paper.

Acknowledgement

Thanks to AJE and Charlesworth Group for the language polishing.

Appendix A. Supplementary data

Supplementary data to this article can be found online at https://doi.org/10.1016/j.heliyon.2024.e28236.

References

[1] M.C. Boelens, T.J. Wu, B.Y. Nabet, B. Xu, Y. Qiu, T. Yoon, et al., Exosome transfer from stromal to breast cancer cells regulates therapy resistance pathways, Cell 159 (2014) 499–513. https://10.1016/j.cell.2014.09.051.
[2] N.I. Nissen, M. Karsdal, N. Willumsen, Collagens and Cancer associated fibroblasts in the reactive stroma and its relation to Cancer biology, J. Exp. Clin. Cancer Res. 38 (2019) 115. https://10.1186/s13046-019-1110-6.
[3] S. Galland, I. Stamenkovic, Mesenchymal stromal cells in cancer: a review of their immunomodulatory functions and dual effects on tumor progression, J. Pathol. 250 (2020) 555–572. https://10.1002/path.5357.
[4] R.D. Schreiber, L.J. Old, M.J. Smyth, Cancer immunoediting: integrating immunity's roles in cancer suppression and promotion, Science 331 (2011) 1565–1570. https://10.1126/science.1203486.
[5] D.V. Sawant, H. Yano, M. Chikina, Q. Zhang, M. Liao, C. Liu, et al., Adaptive plasticity of IL-10(+) and IL-35(+) T(reg) cells cooperatively promotes tumor T cell exhaustion, Nat. Immunol. 20 (2019) 724–735. https://10.1038/s41590-019-0346-9.
[6] N.P. Kristensen, C. Heeke, S.A. Tvingsholm, A. Borch, A. Draghi, M.D. Crowther, et al., Neoantigen-reactive CD8+ T cells affect clinical outcome of adoptive cell therapy with tumor-infiltrating lymphocytes in melanoma, J. Clin. Invest. 132 (2022). https://10.1172/jci150535.
[7] S. Grisaru-Tal, M.E. Rothenberg, A. Munitz, Eosinophil-lymphocyte interactions in the tumor microenvironment and cancer immunotherapy, Nat. Immunol. 23 (2022) 1309–1316. https://10.1038/s41590-022-01291-2.
[8] X. Chen, E. Song, Turning foes to friends: targeting cancer-associated fibroblasts, Nat. Rev. Drug Discov. 18 (2019) 99–115. https://10.1038/s41573-018-0004-1.
[9] X. Mao, J. Xu, W. Wang, C. Liang, J. Hua, J. Liu, et al., Crosstalk between cancer-associated fibroblasts and immune cells in the tumor microenvironment: new findings and future perspectives, Mol. Cancer 20 (2021) 131. https://10.1186/s12943-021-01428-1.
[10] H. Hu, Z. Piotrowska, P.J. Hare, H. Chen, H.E. Mulvey, A. Mayfield, et al., Three subtypes of lung cancer fibroblasts define distinct therapeutic paradigms, Cancer Cell 39 (2021) 1531–1547.e1510. https://10.1016/j.ccell.2021.09.003.
[11] Y. Lin, Q. Cai, Y. Chen, T. Shi, W. Liu, L. Mao, et al., CAFs shape myeloid-derived suppressor cells to promote stemness of intrahepatic cholangiocarcinoma through 5-lipoxygenase, Hepatology 75 (2022) 28–42. https://10.1002/hep.32099.
[12] A. Christofides, L. Strauss, A. Yeo, C. Cao, A. Charest, V.A. Boussiotis, The complex role of tumor-infiltrating macrophages, Nat. Immunol. 23 (2022) 1148–1156. https://10.1038/s41590-022-01267-2.
[13] N.K. Altorki, G.J. Markowitz, D. Gao, J.L. Port, A. Saxena, B. Stiles, et al., The lung microenvironment: an important regulator of tumour growth and metastasis, Nat. Rev. Cancer 19 (2019) 9–31. https://10.1038/s41568-018-0081-9.
[14] H.W. Cheng, Y.F. Chen, J.M. Wong, C.W. Weng, H.Y. Chen, S.L. Yu, et al., Cancer cells increase endothelial cell tube formation and survival by activating the PI3K/Akt signalling pathway, J. Exp. Clin. Cancer Res. 36 (2017) 27. https://10.1186/s13046-017-0495-3.
[15] F. Tang, C. Barbacioru, Y. Wang, E. Nordman, C. Lee, N. Xu, et al., mRNA-Seq whole-transcriptome analysis of a single cell, Nat. Methods 6 (2009) 377–382. https://10.1038/nmeth.1315.
[16] C. Gawad, W. Koh, S.R. Quake, Single-cell genome sequencing: current state of the science, Nat. Rev. Genet. 17 (2016) 175–188. https://10.1038/nrg.2015.16.
[17] D. Lambrechts, E. Wauters, B. Boeckx, S. Aibar, D. Nittner, O. Burton, et al., Phenotype molding of stromal cells in the lung tumor microenvironment, Nat Med 24 (2018) 1277–1289. https://10.1038/s41591-018-0096-5.
[18] N. Kim, H.K. Kim, K. Lee, Y. Hong, J.H. Cho, J.W. Choi, et al., Single-cell RNA sequencing demonstrates the molecular and cellular reprogramming of metastatic lung adenocarcinoma, Nat. Commun. 11 (2020) 2285. https://10.1038/s41467-020-16164-1.
[19] X. Wang, Z. Chen, J. Xu, S. Tang, N. An, L. Jiang, et al., SLC1A1-mediated cellular and mitochondrial influx of R-2-hydroxyglutarate in vascular endothelial cells promotes tumor angiogenesis in IDH1-mutant solid tumors, Cell Res. 32 (2022) 638–658. https://10.1038/s41422-022-00650-w.
[20] K. Mittal, J. Ebos, B. Rini, Angiogenesis and the tumor microenvironment: vascular endothelial growth factor and beyond, Semin. Oncol. 41 (2014) 235–251. https://10.1053/j.seminoncol.2014.02.007.
[21] J.C. Schupp, T.S. Adams, C. Cosme, M.S.B. Raredon, Y. Yuan, N. Omote, et al., Integrated single-cell atlas of endothelial cells of the human lung, Circulation 144 (2021) 286–302. https://10.1161/circulationaha.120.052318.
[22] A. Gillich, F. Zhang, C.G. Farmer, K.J. Travaglini, S.Y. Tan, M. Gu, et al., Capillary cell-type specialization in the alveolus, Nature 586 (2020) 785–789. https://10.1038/s41586-020-2822-7.
[23] H. Jang, Y. Jun, S. Kim, E. Kim, Y. Jung, B.J. Park, et al., FCN3 functions as a tumor suppressor of lung adenocarcinoma through induction of endoplasmic reticulum stress, Cell Death Dis. 12 (2021) 407. https://10.1038/s41419-021-03675-y.

[24] F. Wei, Y. Ge, W. Li, X. Wang, B. Chen, Role of endothelin receptor type B (EDNRB) in lung adenocarcinoma, Thorac Cancer 11 (2020) 1885–1890. https://10.1111/1759-7714.13474.
[25] S. Neri, G. Ishii, H. Hashimoto, T. Kuwata, K. Nagai, H. Date, et al., Podoplanin-expressing cancer-associated fibroblasts lead and enhance the local invasion of cancer cells in lung adenocarcinoma, Int. J. Cancer 137 (2015) 784–796. https://10.1002/ijc.29464.
[26] D. Yin, Y. Jia, Y. Yu, M.V. Brock, J.G. Herman, C. Han, et al., SOX17 methylation inhibits its antagonism of Wnt signaling pathway in lung cancer, Discov. Med. 14 (2012) 33–40.
[27] R. Satija, J.A. Farrell, D. Gennert, A.F. Schier, A. Regev, Spatial reconstruction of single-cell gene expression data, Nat. Biotechnol. 33 (2015) 495–502. https://10.1038/nbt.3192.
[28] D. Aran, A.P. Looney, L. Liu, E. Wu, V. Fong, A. Hsu, et al., Reference-based analysis of lung single-cell sequencing reveals a transitional profibrotic macrophage, Nat. Immunol. 20 (2019) 163–172. https://10.1038/s41590-018-0276-y.
[29] S. Hänzelmann, R. Castelo, J. Guinney, GSVA: gene set variation analysis for microarray and RNA-seq data, BMC Bioinf. 14 (2013) 7. https://10.1186/1471-2105-14-7.
[30] K. Slowikowski, Ggrepel: automatically position non-overlapping text labels with 'ggplot2', R package version 0.9.1 (2023).
[31] H. Wickham, ggplot2: create elegant data visualisations using the grammar of graphics, R package version 3.3.6 (2016).
[32] M. Efremova, M. Vento-Tormo, S.A. Teichmann, R. Vento-Tormo, CellPhoneDB: inferring cell-cell communication from combined expression of multi-subunit ligand-receptor complexes, Nat. Protoc. 15 (2020) 1484–1506. https://10.1038/s41596-020-0292-x.
[33] K. Troulé, R. Petryszak, M. Prete, J. Cranley, A. Harasty, Z.K. Tuong, S.A. Teichmann, L. Garcia-Alonso, R. Vento-Tormo, CellPhoneDB v5: inferring cell-cell communication from single-cell multiomics data, arXiv preprint arXiv:2311.04567 (2023 Nov 8).
[34] A.M. Newman, C.L. Liu, M.R. Green, A.J. Gentles, W. Feng, Y. Xu, et al., Robust enumeration of cell subsets from tissue expression profiles, Nat. Methods 12 (2015) 453–457. https://10.1038/nmeth.3337.
[35] P. Geeleher, N. Cox, R.S. Huang, pRRophetic: an R package for prediction of clinical chemotherapeutic response from tumor gene expression levels, PLoS One 9 (2014) e107468. https://10.1371/journal.pone.0107468.
[36] J. Folkman, What is the evidence that tumors are angiogenesis dependent? J Natl Cancer Inst 82 (1990) 4–6. https://10.1093/jnci/82.1.4.
[37] I.J. Fidler, L.M. Ellis, The implications of angiogenesis for the biology and therapy of cancer metastasis, Cell 79 (1994) 185–188. https://10.1016/0092-8674(94)90187-2.
[38] S. Goel, D.G. Duda, L. Xu, L.L. Munn, Y. Boucher, D. Fukumura, et al., Normalization of the vasculature for treatment of cancer and other diseases, Physiol. Rev. 91 (2011) 1071–1121. https://10.1152/physrev.00038.2010.
[39] X. Jiang, J. Wang, X. Deng, F. Xiong, S. Zhang, Z. Gong, et al., The role of microenvironment in tumor angiogenesis, J. Exp. Clin. Cancer Res. 39 (2020) 204. https://10.1186/s13046-020-01709-5.
[40] X. Wang, A. Freire Valls, G. Schermann, Y. Shen, I.M. Moya, L. Castro, et al., YAP/TAZ orchestrate VEGF signaling during developmental angiogenesis, Dev. Cell 42 (2017) 462–478.e467. https://10.1016/j.devcel.2017.08.002.
[41] N.S. Merle, S.E. Church, V. Fremeaux-Bacchi, L.T. Roumenina, Complement system Part I - molecular mechanisms of activation and regulation, Front. Immunol. 6 (2015) 262. https://10.3389/fimmu.2015.00262.
[42] E.S. Reis, D.C. Mastellos, D. Ricklin, A. Mantovani, J.D. Lambris, Complement in cancer: untangling an intricate relationship, Nat. Rev. Immunol. 18 (2018) 5–18. https://10.1038/nri.2017.97.
[43] S. Tsukita, M. Furuse, M. Itoh, Multifunctional strands in tight junctions, Nat. Rev. Mol. Cell Biol. 2 (2001) 285–293. https://10.1038/35067088.
[44] S. Nakamura, K. Irie, H. Tanaka, K. Nishikawa, H. Suzuki, Y. Saitoh, et al., Morphologic determinant of tight junctions revealed by claudin-3 structures, Nat. Commun. 10 (2019) 816. https://10.1038/s41467-019-08760-7.
[45] S. Tsukita, H. Tanaka, A. Tamura, The claudins: from tight junctions to biological systems, Trends Biochem. Sci. 44 (2019) 141–152. https://10.1016/j.tibs.2018.09.008.
[46] H. Takahashi, M. Oshi, L. Yan, I. Endo, K. Takabe, Gastric cancer with enhanced apical junction pathway has increased metastatic potential and worse clinical outcomes, Am. J. Cancer Res. 12 (2022) 2146–2159.
[47] A.C. Joerger, A.R. Fersht, The p53 pathway: origins, inactivation in cancer, and emerging therapeutic approaches, Annu. Rev. Biochem. 85 (2016) 375–404. https://10.1146/annurev-biochem-060815-014710.
[48] L.A. Donehower, T. Soussi, A. Korkut, Y. Liu, A. Schultz, M. Cardenas, et al., Integrated analysis of TP53 gene and pathway alterations in the cancer genome atlas, Cell Rep. 28 (2019) 1370–1384.e1375. https://10.1016/j.celrep.2019.07.001.
[49] A. Giatromanolaki, M.I. Koukourakis, S. Kakolyris, H. Turley, K. O'Byrne, P.A. Scott, et al., Vascular endothelial growth factor, wild-type p53, and angiogenesis in early operable non-small cell lung cancer, Clin. Cancer Res. 4 (1998) 3017–3024.
[50] Y. Yoshioka, S. Shimizu, T. Ito, M. Taniguchi, M. Nomura, T. Nishida, et al., p53 inhibits vascular endothelial growth factor expression in solid tumor, J. Surg. Res. 174 (2012) 291–297. https://10.1016/j.jss.2010.12.028.
[51] S. Wang, A. Raybuck, E. Shiuan, S.H. Cho, Q. Wang, D.M. Brantley-Sieders, et al., Selective inhibition of mTORC1 in tumor vessels increases antitumor immunity, JCI Insight 5 (2020). https://10.1172/jci.insight.139237.
[52] L. He, J. Chen, F. Xu, J. Li, J. Li, Prognostic implication of a metabolism-associated gene signature in lung adenocarcinoma, Mol Ther Oncolytics 19 (2020) 265–277. https://10.1016/j.omto.2020.09.011.
[53] J. Li, H. Wang, Z. Li, C. Zhang, C. Zhang, C. Li, et al., A 5-gene signature is closely related to tumor immune microenvironment and predicts the prognosis of patients with non-small cell lung cancer, BioMed Res. Int. 2020 (2020) 2147397. https://10.1155/2020/2147397.
[54] Y. Yao, T. Zhang, L. Qi, R. Liu, G. Liu, J. Li, et al., Identification of four genes as prognosis signatures in lung adenocarcinoma microenvironment, Pharmgenomics Pers Med 14 (2021) 15–26. https://10.2147/pgpm.S283414.
[55] M.P. Jansen, L. Sas, A.M. Sieuwerts, C. Van Cauwenberghe, D. Ramirez-Ardila, M. Look, et al., Decreased expression of ABAT and STC2 hallmarks ER-positive inflammatory breast cancer and endocrine therapy resistance in advanced disease, Mol. Oncol. 9 (2015) 1218–1233. https://10.1016/j.molonc.2015.02.006.
[56] H. Han, S. Zhou, G. Chen, Y. Lu, H. Lin, ABAT targeted by miR-183-5p regulates cell functions in liver cancer, Int. J. Biochem. Cell Biol. 141 (2021) 106116. https://10.1016/j.biocel.2021.106116.
[57] B. Stankovic, H.A.K. Bjørhovde, R. Skarshaug, H. Aamodt, A. Frafjord, E. Müller, et al., Immune cell composition in human non-small cell lung cancer, Front. Immunol. 9 (2018) 3101. https://10.3389/fimmu.2018.03101.
[58] S. Wang, P. Yuan, B. Mao, N. Li, J. Ying, X. Tao, et al., Genomic features and tumor immune microenvironment alteration in NSCLC treated with neoadjuvant PD-1 blockade, npj Precis. Oncol. 6 (2022) 2. https://10.1038/s41698-021-00244-6.
[59] R. Mu, H. Liu, S. Luo, E.F. Patz Jr., C. Glass, L. Su, et al., Genetic variants of CHEK1, PRIM2 and CDK6 in the mitotic phase-related pathway are associated with nonsmall cell lung cancer survival, Int. J. Cancer 149 (2021) 1302–1312. https://10.1002/ijc.33702.
[60] K. She, W. Yang, M. Li, W. Xiong, M. Zhou, FAIM2 promotes non-small cell lung cancer cell growth and bone metastasis by activating the wnt/β-catenin pathway, Front. Oncol. 11 (2021) 690142. https://10.3389/fonc.2021.690142.
[61] Y. Ito, K. Oshinden, N. Kutsuzawa, C. Kohno, S. Isaki, K. Yokoyama, et al., Heat-Not-Burn cigarette induces oxidative stress response in primary rat alveolar epithelial cells, PLoS One 15 (2020) e0242789. https://10.1371/journal.pone.0242789.
[62] Z. Wang, P. Lei, Z. Li, X. Han, F. Yang, T. Su, et al., Proteomic and phosphoproteomic analyses reveal the oncogenic role of PTK7-NDRG1 Axis in non-small-cell lung cancer cell resistance to AZD9291, ACS Chem. Biol. 17 (2022) 2849–2862. https://10.1021/acschembio.2c00479.
[63] K. Azuma, A. Kawahara, S. Hattori, T. Taira, J. Tsurutani, K. Watari, et al., NDRG1/Cap43/Drg-1 may predict tumor angiogenesis and poor outcome in patients with lung cancer, J. Thorac. Oncol. 7 (2012) 779–789. https://10.1097/JTO.0b013e31824c92b4.
[64] A. Komatsu, K. Nagasaki, M. Fujimori, J. Amano, Y. Miki, Identification of novel deletion polymorphisms in breast cancer, Int. J. Oncol. 33 (2008) 261–270.
[65] H. Ju, B. Lim, M. Kim, Y.S. Kim, W.H. Kim, C. Ihm, et al., A regulatory polymorphism at position -309 in PTPRCAP is associated with susceptibility to diffuse-type gastric cancer and gene expression, Neoplasia 11 (2009) 1340–1347. https://10.1593/neo.91132.